SIW Multibeam Array for 5G Mobile Devices

**QING-LING YANG[1], YONG-LING BAN[1], KAI KANG[1], (Member, IEEE),
CHOW-YEN-DESMOND SIM[2], (Senior Member, IEEE),
AND GANG WU[3], (Member, IEEE)**

[1]School of Electronic Engineering, University of Electronic Science and Technology of China, Chengdu 611731, China
[2]Department of Electrical Engineering, Feng Chia University, Taichung 40724, Taiwan
[3]National Key Laboratory of Science and Technology on Communication, University of Electronic Science and Technology of China, Chengdu 611731, China

Corresponding author: Y.-L. Ban (byl@uestc.edu.cn)

ABSTRACT This paper presents a substrate integrated waveguide (SIW) multibeam slot array operating at ∼30 GHz for future 5G mobile terminal applications. The multibeam forming network is realized with a Butler matrix that is composed of hybrid couplers, crossovers, and phase shifters (135° and 0°). The crossovers are formed with two cascaded hybrid couplers. In the design of 135° and 0° phase shifters, the phase compensation technique is employed. The slot array is a 2 × 4 type, in which each column has two slot elements that are longitudinally staggered with respect to one another (in half-wavelength). In addition, mutual couplings reduction techniques applied in the proposed slot array are also discussed. The SIW technique is adopted in case for the related components, as it can be highly integrated in mmWave circuits at low fabrication cost and has low profile characteristics. The overall dimension of the SIW multibeam slot array (including the Butler matrix feeding network) is $72 \times 27.4 \times 0.508$ mm^3, and the total area of the slot array is only 10.1×20.4 mm^2. The measured 10 dB bandwidth was 28–32 GHz, and the measured gains at 30 GHz for each port were 10.8, 12.1, 12, and 11 dBi. The proposed slot array also possesses wide angle coverage of ∼40° with good steerable radiation.

INDEX TERMS 5G, butler matrix, mobile terminals, substrate integrated waveguide (SIW), millimeter wave.

I. INTRODUCTION

There is a huge demand at the moment to increase the data rate and data traffic for present fourth generation (4G) mobile communication systems. Because the spectrums bandwidth below 6 GHz are now used very intensively by the mobile network operators, there will be an increasing need to unlock new spectrum bands beyond 6 GHz (up to 100 GHz) for mobile user, especially during the migration from 4G LTE (Long Term Evolution) to the fifth generation (5G) communication systems. Therefore, it have been widely speculated that bands at millimeter-Wave (mmWave, 30–100 GHz) maybe a good candidate, considering the large bandwidths that could be exploited for improving the channel capacity, as well as very high data-transfer rate that the user may experience [1], [2]. However, according to Friis formula [3], increasing the frequency will result in aggravating the path loss. One of the solutions is to increase the transmission distance by enlarging the antenna's aperture. Even though increasing the aperture size can improve the antenna gain, the downside is

a narrow beamwidth with reduced coverage areas. Therefore, to achieve both high gain and wide coverage areas for possible 5G mobile terminals, the use of phased array and multibeam schemes are promising candidates at the moment. As reported in [4] and [5], phased array is adopted to achieve multiple beams and good coverage efficiency, however, the costly T/R modules and complexity of the hardware implementation of phased array are some of the significant factors that have to be taken into consideration. For practical use and large-scale application, it is highly desirable that the feeding networks are low in fabrication cost and low in profile.

Theoretically, the multibeam system is originated from the phased array system, because its beams' directions are also dependent on the given phase, and the differences between them are their implementation and applications. The multibeam schemes have already been implemented in WLAN [6], base stations [7], satellite communications [8] and even automotive radars [9]. Among them, satellite communications and automotive radars have used mmWave. As for
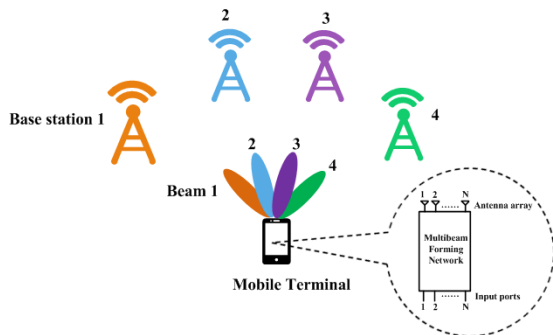
FIGURE 1. Multibeam operation principle in 5G communication systems.

mmWave applications, it could be used in mobile terminal due to its small-size advantages. Fig. 1 describes how the multibeam operation works in 5G communication systems. The beams generated by beamforming network in the mobile terminal can realize wide coverage areas, and each beam will be responded by a base station nearby. Thus, in this 5G communication system, mobile terminals with multibeams can improve both channel capacity and coverage efficiency. However, as mentioned earlier, severe path loss will incur in mmWave bands, and the effective transmission distance between the mobile terminal and base stations will be significantly reduced. Thus, in order for the base stations to maintain real-time links with the mobile terminal, one of the solutions is to increase the number of base stations, but that will lead to increasing cost for the mobile network operators. On the other hand, designing a multibeam array antenna for mobile terminal with wide coverage area and high gain is a good and least expensive option.

In this paper, a multibeam array antenna at mmWave (approximately 30 GHz) that can exhibit good gain (>10.8 dBi), wide angle coverage (approximately 140°), and good steerable radiation (multibeam) is proposed for future possible 5G mobile terminals. The proposed array is fed by a Butler matrix feeding network (BMFN) incorporate with SIW technology, because the radiation loss can be kept at an insignificant level. Slot antenna design is selected in this work as the main radiating elements for the array, because it is very convenient to be etched on SIW structure. This paper is organized as follows: Section II introduces the Butler matrix operating at approximately 30 GHz, and covers the design process of its related components. At the end of this section, its cascaded simulations are provided. Section III presents the radiating array design. Section IV presents the physical fabrication and measured results of the designed multibeam system that include scattering parameters, scanning properties and realized gains. Concluding remarks are given in Section V.

II. BUTLER MATRIX DESIGN

Compared with other beamformers like Nolen matrix [10], Blass matrix [11], [12], reflector lens [13] and

Rotman lens [14] counterparts, the Butler matrix is the most popular choice, because it utilizes minimum number of components and has relatively simple configuration. Furthermore, it can also be exploited to provide the necessary bandwidth, scanning capabilities and beamwidth. By taking advantage of its orthogonal beam property, the Butler matrix can produce or receive multiple beams simultaneously, which will greatly improve the channel capacity and scanning coverage. In general, a Butler matrix consists of hybrid couplers, crossovers and phase shifters, and it is essentially a device that functions as power dividing and phase shifting to realize the required amplitude distribution and specified identical phase difference between output ports [15]. As a result, antenna array fed by Butler matrix will produce multibeams with different directions. The implementation of BMFN has many forms, such as those designs without crossovers [16] or in multilayers [17].
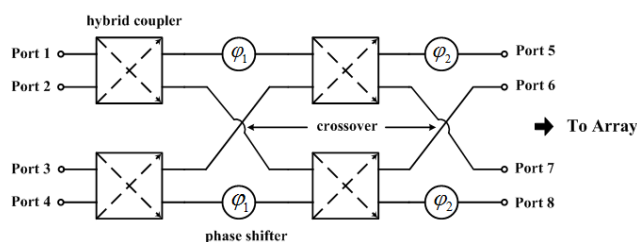

FIGURE 2. The block diagram of proposed Butler matrix feeding network.

In this work, the Butler matrix is composed of four hybrid couplers, two crossovers and two pairs of phase shifters. For ease in fabrication, all of these components are geometrically arranged in the same layer. The detail block diagram of proposed BMFN is shown in Fig. 2. The four feeding ports of Butler matrix are Ports 1–4, and its corresponding output ports connecting to the antenna array are Ports 5–8. Here, when an RF signal is fed into one of the feeding ports, the other feeding ports will be isolated. Besides receiving equal RF signal power (−6 dB) from the feeding port, the four output ports will also exhibit uniform phase differences between adjacent ports.

TABLE 1. Relationships between feeding ports and output phase differences.

Feeding port	Port 1	Port 2	Port 3	Port 4
Output phase difference	135°	−45°	45°	−135°

In this BMFN design, the φ_1 and φ_2 of phase shifters are set at 135° and 0°, respectively. The relationships between feeding ports and output phase differences are tabulated in Table 1. To ensure that the BMFN can exhibit wideband performances, subsequent wideband components must also be included in the feeding network. The following subsections include the design of all related components and their cascaded simulations. Rogers Duriod 5880 substrate with

thickness of 0.508 mm, loss tangent of 0.0009 and relative dielectric permittivity of 2.2 is used in designs. All related components are implemented and optimized by applying full-wave FEM simulation package, HFSS ver. 15.

A. HYBRID COUPLER AND CROSSOVER

Compared with conventional dielectric-filled rectangular waveguide, the SIW technology [18], [19] comprises the advantage of both planar structure and nonplanar waveguide, and it can be highly integrated in mmWave circuits at low-cost fabrication. Furthermore, in the designs of feeding network and antenna array, due to its low-profile structure characteristics, it can be well adjusted to accommodate the rigorous thickness requirements in 5G mobile terminals. Technically, SIW can be equivalent to dielectric-filled rectangular waveguide [20], as they have shown identical TE_{10}-like mode dispersion. In SIW, the narrow-walls are replaced by periodical metalized vias (0.4 mm diameter and 0.8 mm spacing in our design). As an essential component in Butler matrix, the SIW hybrid coupler has distinct features such as equal power dividing (−3 dB) and accurate 90° phase shift. Topology of the designed SIW hybrid coupler is illustrated in Fig. 3. By adjusting the length and width of the coupling section, the desired power splitting ratio and output phase difference can be achieved.
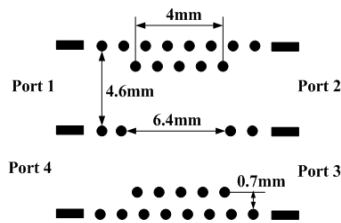
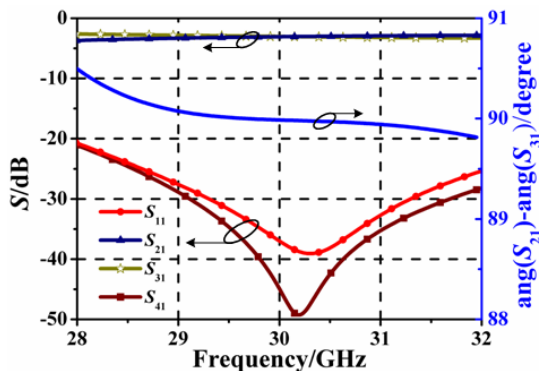**FIGURE 3.** Topology of SIW hybrid coupler.

FIGURE 4. Simulated S-parameters of the hybrid coupler and output phase difference.

Figure 4 shows the simulated scattering parameters over the range from 28 to 32 GHz. In this figure, the directivity and coupling coefficient with a dispersion of ±0.2 dB are centered at −2.9 dB, which means that the −3 dB power

dividing between port 2 and port 3 is approximately obtained in this band. In additional, reflection and mutual coupling levels below −20 dB can also be achieved across the bandwidth. The phase difference between the direct port and coupled port is also illustrated in Fig. 4. It only produces 0.5° dispersion compared with the theoretical 90° phase difference.

Planar crossover can be formed with two cascaded hybrid couplers [6]. In general, a well-designed hybrid coupler will have good crossover performance, and the proposed one in this case can be validated by observing the simulated scattering parameters shown in Fig. 5.
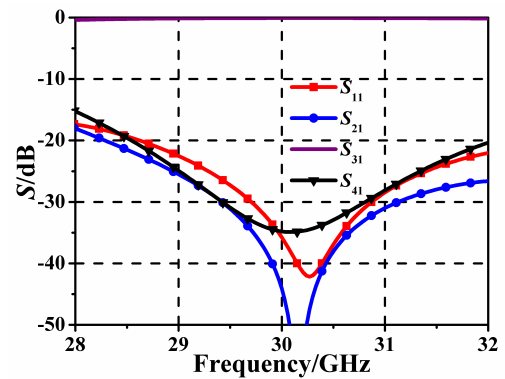
FIGURE 5. Simulated S-parameters of the crossover.

B. PHASE SHIFTERS

Phase shifters are critical components in realizing the specified fixed output phase differences. In theory, by varying the width of SIW, its corresponding phase constant will change; follow by producing a phase shift. This is one of the basic skills in designing phase shifters, even though phase shifting can also be obtained by using delay-line or other approaches. In this case, the first approach is to narrow the width of SIW, so as to obtain 135° phase shifting in the design. Fig. 6(a) shows the configuration and dimensions of the designed 135° phase shifter. Both the 135° phase shifter and the following 0° phase shifter are achieved by taking the phase introduced by the crossover reported in [21]. The phase compensation technique reported in [22] is also employed here, which is critical for reducing phase imbalance in multibeam forming networks. However, the simulation illustrates that it can be difficult to design the 0° phase shifter by changing
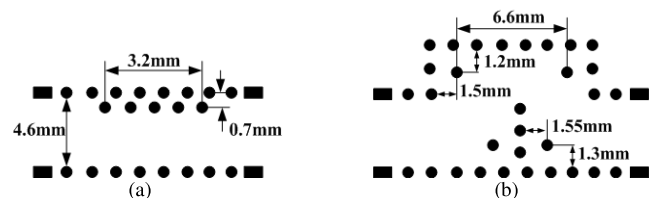
FIGURE 6. Topology and detailed dimensions of phase shifters. (a) 135 degree phase shifter. (b) 0 degree phase shifter.

the SIW width, because the phase of referenced crossover cannot be tuned easily. By observing [23] that applies the method of meandering SIW path and inserting inductive posts to its corners, similar topology is also applied to the 0° phase shifter of this work, and its detailed dimensions are shown in Fig. 6(b).

Figure 7 shows that both 135° and 0° phase shifters can achieve wide bandwidth characteristics ($S_{11} < -20$ dB) across 28 to 32 GHz band. For the 135° phase shifter, the simulated phase values for 28–32 GHz are $135° \pm 5°$. Within the range 28–30 GHz, the 0° phase shifter shows phase shifting of near zero, and in the range 30–32 GHz, its corresponding simulated phase shifting have a slight offset of $3.5° \pm 3.5°$.
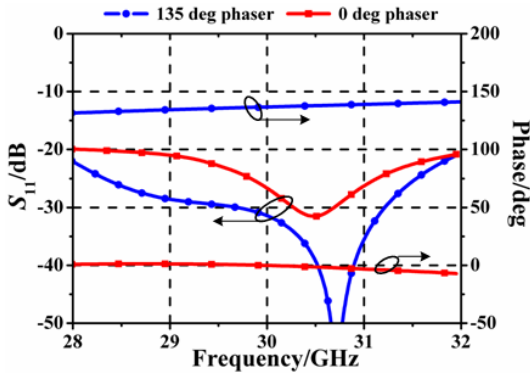
FIGURE 7. Simulated reflections and phases of 135 degree and 0 degree phase shifters.
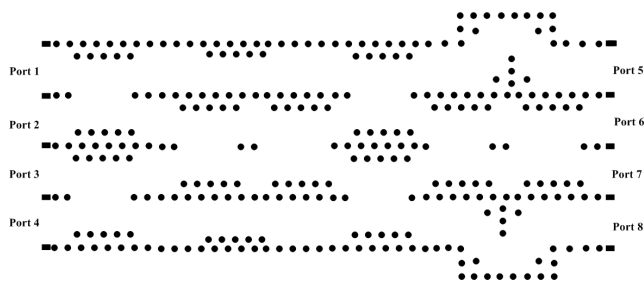
FIGURE 8. Topology of SIW Butler matrix.

C. CASCADED SIMULATION OF WIDEBAND COMPONENTS

As the design of all wideband components of Butler matrix have been clearly discussed, the topology of the cascaded components is now shown in Fig. 8, and its overall dimension is $55.62 \times 27.4 \times 0.508$ mm³. As depicted in Fig. 9(a), the reflection and coupling levels of port 1 are better than -20 dB over the range 28.8–31.3 GHz. As for port 2, the reflection and coupling levels across 29.1–31.4 GHz are better than -20 dB, as depicted in Fig. 9(b). By further observing Fig. 8, the simulated transmission coefficients of port 1 and port 2 (as input ports) are -7.0 ± 0.8 dB and -7.0 ± 2.8 dB, respectively. In particular, the beamformer shows better results over the higher frequency range 30–32 GHz, as the transmission coefficients are centered at -6.3 dB with only 0.3 dB of dispersion.
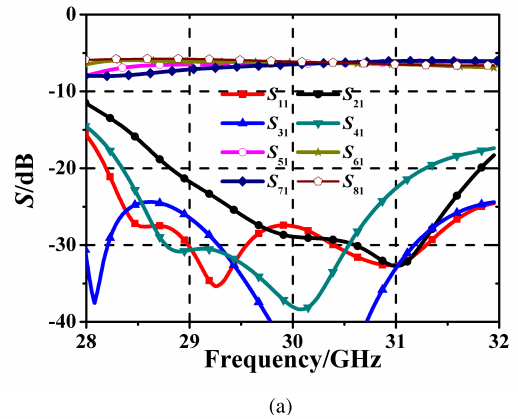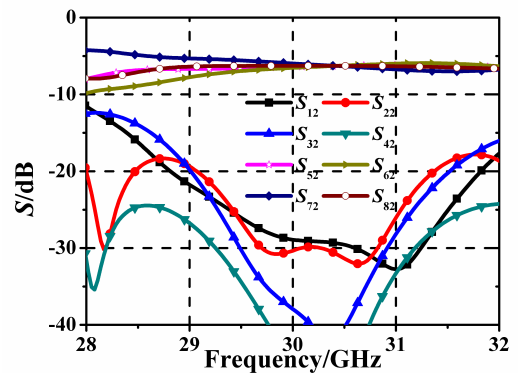
FIGURE 9. Simulated S-parameters of the SIW Butler matrix. (a) S-parameters with port 1 excited. (b) S-parameters with port 2 excited.
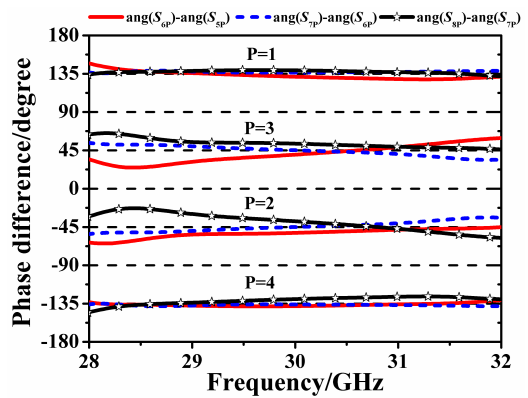
FIGURE 10. Output phase differences. (P=1, port 1 excited), (P=2, port 2 excited), (P=3, port 3 excited), and (P=4, port 4 excited). One port will be excited at each time.

Figure 10 reveals the simulated phase differences of two adjacent output ports, namely, $ang(S_{6P}) - ang(S_{5P})$, $ang(S_{7P}) - ang(S_{6P})$, and $ang(S_{8P}) - ang(S_{7P})$. Here, when one of the feeding ports is excited (P=1 to P=4), the other three feeding ports are with 50Ω termination. Theoretically, the relative phases between two adjacent output ports are 135°, $-45°$, 45° and $-135°$, for ports 1, 2, 3, and 4 excitation. At 30 GHz, for P=1 or P=4, the simulated phase errors
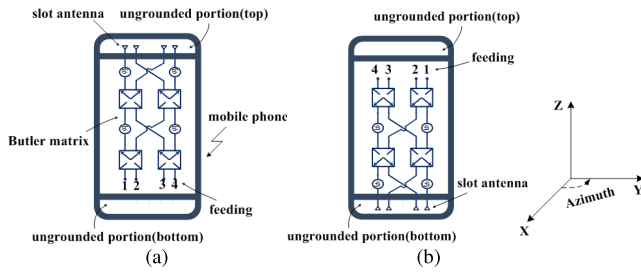
FIGURE 11. Placement of multibeam slot array in mobile phone. (a) slot array placed at the top of mobile phone. (b) slot array placed at the bottom of mobile phone.

FIGURE 12. Topology of SIW slot element and slot array. (a) Branch of slot antenna. (b) 2 × 4 slot array. *L* = 20.4mm, *W* = 10.1mm.

fall within 5° and vary to about 10° across 30–32 GHz. For P=2 or P=3 at 30 GHz, the simulated phase error is approximately 6°. Notably, in the lower band, maximum phase errors of approximately 21° are also observed.

III. ANTENNA ARRAY

Due to its excellent polarization purity and very low profile characteristics, slot antenna design incorporated into an array type has been widely used in mmWave application field. It is well known that the main antenna of a 4G LTE mobile phone is usually mounted in the ungrounded portion, in which the common width allocated is approximately 10 mm, or 20 mm at most. Due to the fact that mobile phone users prefer their phone to have higher screen-to-body ratio or thinner bezel, these limitations will restrict the dimension of the main antenna, not to mention its design flexibility. Therefore, within the restricted spaces allocated for the mobile phone antenna, it is difficult for antennas' engineer to arrange a certain number of slot antennas in the longitudinal direction of radiation aperture. However, at 30 GHz, the wavelength in the SIW is only 9.9 mm, and because of that, two slot elements can be longitudinally staggered (in half-wavelength) in the ungrounded portion. As shown in Figs. 11(a) and (b), the slot antenna can be placed in the top or bottom unground portion of the mobile phones, respectively. Figs. 12(a) and (b) show the topology of the single branch SIW slot antenna and its corresponding 2 × 4 slot array, respectively.

In planar slot array, mutual coupling is detrimental to port isolation, and will spoil its overall performances. Many approaches have been developed to mitigate the effect of mutual coupling between antennas in neighboring row, such as using perfectly conducting fences [24] or electromagnetic band gap (EBG) [25], etc. However, with these approaches, the mutual coupling only reduced by a few decibels, at the cost of owning a complex construction. To achieve simplicity and practicability, the mutual couplings are reduced to a relative low level by optimizing the slot lengths and offsets, as shown in Fig. 13. Table 2 presents optimized parameters of the branch SIW slot antenna slotted as shown in Fig. 12(a). In this case, it is noteworthy that the slot array arrangement has higher gain and best fit the restricted size specifications of mobile phone. From the simulation, the single branch slot
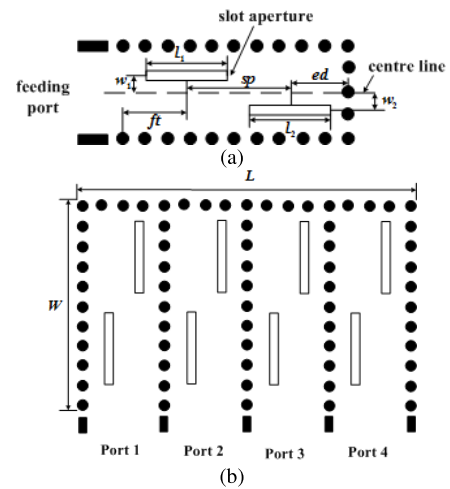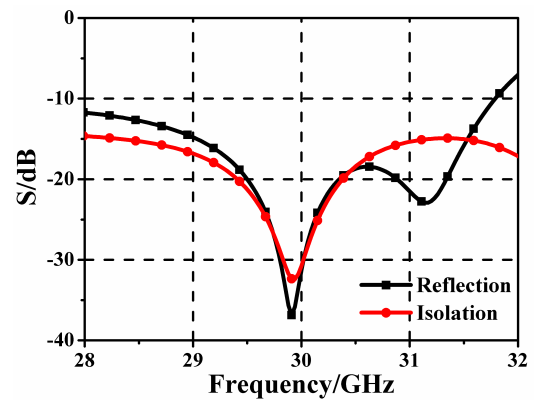

FIGURE 13. Simulated isolation and reflection of slot array.

TABLE 2. Detailed dimensions of the optimized slots (Units: mm).

l_1	l_2	$offset_1$	$offset_2$	sp	ft	ed
4.46	4.61	-0.51	0.3	4.96	4.96	2.48

antenna (two slot elements) at 30 GHz can exhibit gain of up to 8.6 dBi. Therefore, in principle, the maximum gain of it corresponding 2 × 4 slot array type can be up to 14.6 dBi.

At different feeding port excitation, uniform amplitudes with difference phase distributions can be achieved in the output ports, which allow the designed slot array to radiate beams tilted in different angles. Theoretically, beam pointing angles β can be calculated by applying the formula as follow [26]:

$$\beta = 90° - \arccos\left(-\frac{\alpha}{kd}\right)$$

whereby α is the phase difference, k is the wave-number, and d is the element spacing. By setting the α values to $\pm\pi/4$ and $\pm3\pi/4$, its corresponding calculated pointing angles will be $\pm14°$ and $\pm48°$, respectively, while its simulated ones

are $\pm13.8°$ and $\pm48.2°$. The simulated radiation patterns of proposed slot array shown in Fig. 14 validate the aforementioned calculation.
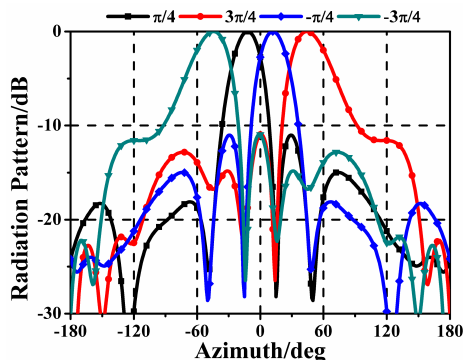

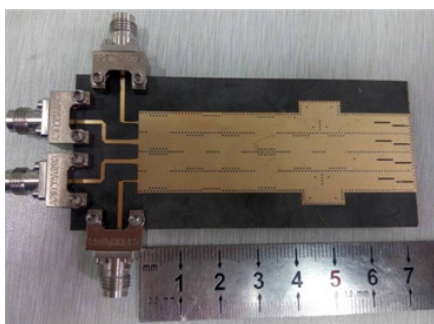**FIGURE 14.** Simulated radiation patterns of the slot array.

FIGURE 15. Photograph of the fabricated SIW multibeam slot array.

IV. FABRICATION AND MEASUREMENTS

The proposed 4×4 Butler matrix multibeam array was fabricated and tested for verification. The whole circuit was implemented on Rogers 5880 dielectric substrate, as shown in Fig. 15. Its overall dimension is $72 \times 27.4 \times 0.508$ mm^3, which is smaller than most of the present mobile phones available at the moment. From the simulation, the slightly smaller ground portion does not introduce much effect on the overall performances, as the electromagnetic wave is completely isolated in the SIW structure and the radiated counterpart is also not able to pose too much influence. The measurements on scattering parameters, gain and radiation patterns were accomplished by using Agilent E8363B Network Analyzer, and also the anechoic chamber system, as shown in Fig. 16. Except for the port under test, the unused ports are terminated by 50Ω broadband matching loads through 2.40 mm end launch connectors. In order to provide better impedance matching and electrical connecting, the microstrip transition that sandwiched between the connector and SIW has been carefully designed.

Fig. 17(a) shows the simulated and measured reflection coefficients of proposed multibeam slot array when every port was fed. Between 28 GHz and 32 GHz, both the simulated
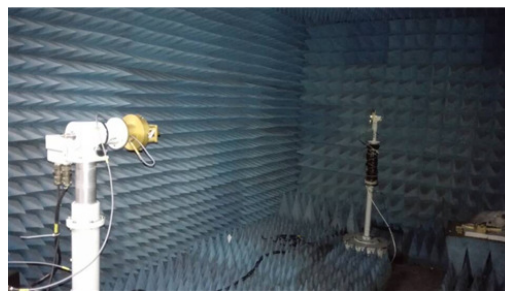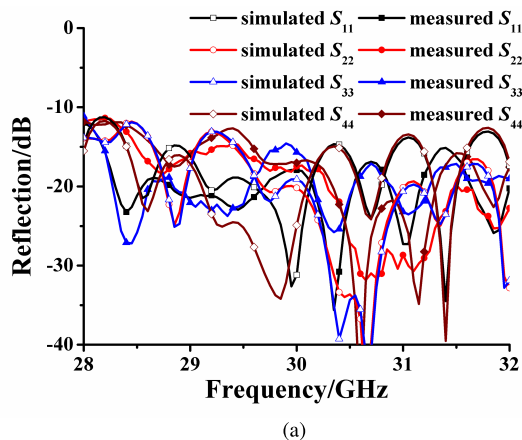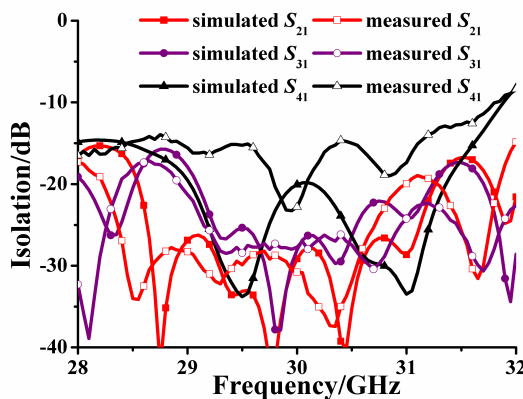

FIGURE 16. Prototype of the fabricated multibeam slot array under test.

(a)

(b)

FIGURE 17. Measured S-parameters of fabricated multibeam slot array. (a) Measured reflection coefficients of each port. (b) Simulated and measured isolations of port 1 and other ports.

and measured reflection coefficients were below -12 dB. The isolations of port 1 and other ports (2–4) are shown in Fig. 17(b).

The measured E-plane radiation patterns across 28–32 GHz for input ports 1 and 2 excited are shown in Figs. 18(a) and (b), respectively. Here, the radiation patterns vary slightly with frequency, except for the side lobe levels (SLLs). For the proposed antenna array fed by a 4×4 Butler matrix beamformer, the optimal SLL is -13 dB in theory. However, the simulated and measured results show
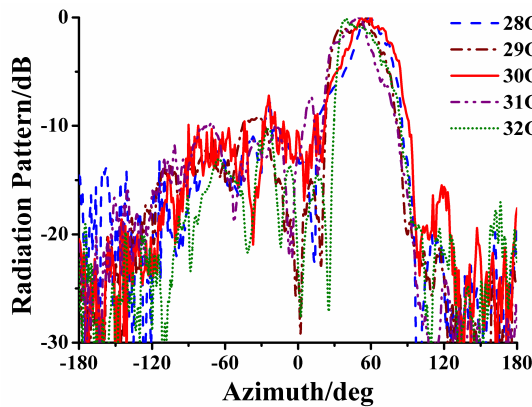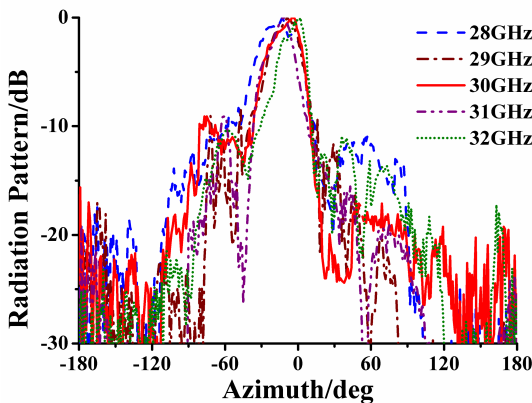
FIGURE 18. Radiation patterns across 28–32 GHz. (a) Port 1 excited. (b) Port 2 excited.

FIGURE 19. Radiation patterns at 30 GHz for each excited port.
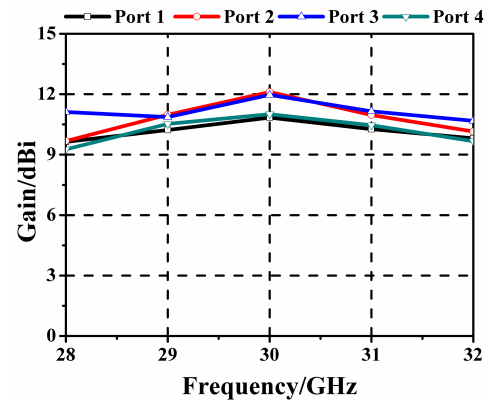
FIGURE 20. Measured gains for each port excited.

that it cannot be better than −10 dB, because it is nearly impossible to ensure that the incident powers of antennas are uniform. This phenomenon may be due to various reflections and losses in different meandering paths, which are usually difficult to accommodate in this case. For symmetry structure, similar radiation patterns can also be achieved when port 3 and port 4 are fed separately.

As discussed in Section III, the edge beams are generated by feeding port 1 and port 4, whereas the center beams are generated by feeding port 2 and port 3. The beam coverage in azimuth plane at 30 GHz for each excited port is illustrated in Fig. 19. It is observed that the main beam directions corresponding to input ports 2 and 3 are ±13°, whereas the input ports 4 and 1 show ±51°. Therefore, the proposed multibeam slot array has shown wide angle coverage of approximately 140° with good steerable radiation. In comparison, the simulated directions are very close to the calculated ones, which could be observed in Section III. By further observing Fig. 19, the −3 dB beamwidths of the two measured ones (±13° and ±51°) were approximately 30° and 40°, respectively.

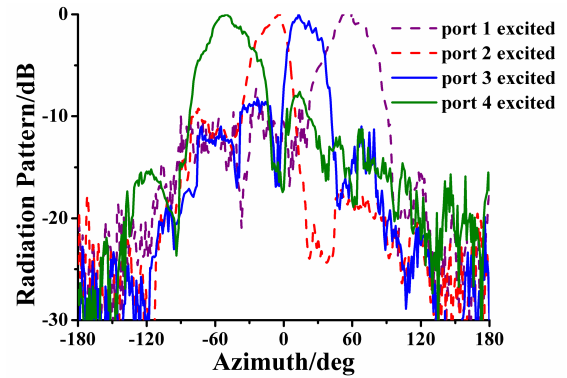The measured gains in the entire bandwidth for ports 1–4 excited are illustrated in Fig. 20. At 30 GHz,

the measured gains at ports 1, 2, 3 and 4 were 10.8, 12.1, 12.0 and 11.0 dBi, respectively. Because the beamwidths excited from port 1 and port 4 are slightly wider (approximately 10°) than port 2 and port 3, as a result, the gains of port 1 and port 4 are slightly (approximately 1 dB) less than those produced by port 2 and port 3. It is worth noting that the gains at both edges (28 and 32 GHz) of entire frequency band have decreased progressively from 30 GHz. These phenomena are mainly due to higher reflection coefficient and more severe imbalance of power amplitude at both edge frequencies. Mismatching of connector to SIW, PCB manufacturing tolerance, measurement error and beam broadening are some of the factors that may contribute to gain uncertainty of each beam with respect to its input port.

V. CONCLUSION

In this paper, an SIW multibeam slot array for future 5G terminal communications is successfully presented, which covers the whole design process including components and array design, fabrication and measurements. At 30 GHz, besides achieving wide beam coverage of approximately 140°, maximum gain of 12.1 dBi was also measured. The four beams generated by each port vary slightly with frequency and maintain at the directions of ±13° and ±51°. The total area of proposed antenna array is only 10.1 × 20.4 mm², and it can be easily fit into the ungrounded portion of a

mobile terminals. Because the proposed SIW multibeam slot array have shown desirable gain, good steerable radiation and compact size that can well satisfy the general requirements in 5G communication system, in view of this, it is a good candidate for future 5G mobile terminals.

REFERENCES

[1] J. G. Andrews *et al.*, "What will 5G be?" *IEEE J. Sel. Areas Commun.*, vol. 32, no. 6, pp. 1065–1082, Jun. 2014.

[2] J. Qiao, X. S. Shen, J. W. Mark, Q. Shen, Y. He, and L. Lei, "Enabling device-to-device communications in millimeter-wave 5G cellular networks," *IEEE Commun. Mag.*, vol. 53, no. 1, pp. 209–215, Jan. 2015.

[3] D. M. Pozar, *Microwave Engineering*. New York, NY, USA: Wiley, 1998, pp. 655–695.

[4] W. Hong, K.-H. Baek, Y. Lee, Y. Kim, and S.-T. Ko, "Study and prototyping of practically large-scale mmWave antenna systems for 5G cellular devices," *IEEE Commun. Mag.*, vol. 52, no. 9, pp. 63–69, Sep. 2014.

[5] J. Helander, K. Zhao, Z. Ying, and D. Sjöberg, "Performance analysis of millimeter-wave phased array antennas in cellular handsets," *IEEE Antennas Wireless Propag. Lett.*, vol. 15, pp. 504–507, Jul. 2015.

[6] C. Collado, A. Grau, and F. De Flaviis, "Dual-band Butler matrix for WLAN systems," in *IEEE MTT-S Int. Microw. Symp. Dig.*, Jun. 2005, pp. 2247–2250.

[7] Y. Li, M. J. Feuerstein, and D. O. Reudink, "Performance evaluation of a cellular base station multibeam antenna," *IEEE Trans. Veh. Technol.*, vol. 46, no. 1, pp. 1–9, Feb. 1997.

[8] Y. M. Cheng, P. Chen, W. Hong, T. Djerafi, and K. Wu, "Substrate-integrated-waveguide beamforming networks and multibeam antenna arrays for low-cost satellite and mobile systems," *IEEE Antennas Propag. Mag.*, vol. 53, no. 6, pp. 18–30, Dec. 2011.

[9] T. Tanizaki, H. Nishida, T. Nishiyama, H. Yamada, K. Sakamoto, and Y. Ishikawa, "Multi-beam automotive radar front end using non-contact cylindrical NRD switch," in *IEEE Int. Microw. Symp. Dig.*, Baltimore, MD, USA, 1998, pp. 521–524.

[10] T. Djerafi, N. J. G. Fonseca, and K. Wu, "Broadband substrate integrated waveguide 4 × 4 Nolen matrix based on coupler delay compensation," *IEEE Trans. Microw. Theory Techn.*, vol. 59, no. 7, pp. 1740–1745, Jul. 2011.

[11] J. Blass, "Multidirectional antenna—A new approach to stacked beams," in *Proc. IRE Int. Conf. Rec.*, vol. 8. 1960, pp. 48–50.

[12] R. C. Hansen, "Multiple-beam antennas," in *Phased Array Antennas*. New York, NY, USA: Wiley, 1998, pp. 330–380.

[13] Y. J. Cheng, W. Hong, and K. Wu, "Millimeter-wave substrate integrated waveguide multibeam antenna based on the parabolic reflector principle," *IEEE Trans. Antennas Propag.*, vol. 56, no. 9, pp. 3055–3058, Sep. 2008.

[14] M. Rajabalian and B. Zakeri, "Optimisation and implementation for a non-focal Rotman lens design," *IET Microw. Antennas Propag.*, vol. 9, no. 9, pp. 982–987, Jun. 2015.

[15] T. Djerafi, N. J. G. Fonseca, and K. Wu, "Design and implementation of a planar 4 × 4 Butler matrix in SIW technology for wideband applications," in *Proc. Eur. Microw. Conf. (EuMC)*, 2010, pp. 910–913.

[16] T. Djerafi and K. Wu, "A low-cost wideband 77-GHz planar butler matrix in SIW technology," *IEEE Trans. Antennas Propag.*, vol. 60, no. 10, pp. 4949–4954, Oct. 2012.

[17] S. Karamzadeh, V. Rafii, M. Kartal, and B. S. Virdee, "Compact and broadband 4 × 4 SIW Butler matrix with phase and magnitude error reduction," *IEEE Antennas Wireless Propag. Lett.*, vol. 25, no. 12, pp. 772–774, Dec. 2015.

[18] Y. J. Cheng, *Substrate Integrated Antennas and Arrays*. London, U.K.: CRC Press, 2015.

[19] S.-J. Park, D.-H. Shin, and S.-O. Park, "Low side-lobe substrate-integrated-waveguide antenna array using broadband unequal feeding network for millimeter-wave handset device," *IEEE Trans. Antennas Propag.*, vol. 64, no. 3, pp. 923–932, Mar. 2016.

[20] W. Che, K. Deng, D. Wang, and Y. L. Chow, "Analytical equivalence between substrate-integrated waveguide and rectangular waveguide," *IET Microw. Antennas Propag.*, vol. 2, no. 1, pp. 35–41, 2008.

[21] K. Tekkouk, J. Hirokawa, R. Sauleau, M. Ettorre, M. Sano, and M. Ando, "Dual-layer ridged waveguide slot array fed by a butler matrix with sidelobe control in the 60-GHz band," *IEEE Trans. Antennas Propag.*, vol. 63, no. 9, pp. 3857–3867, Sep. 2015.

[22] Y. J. Cheng, K. Wu, and W. Hong, "Substrate integrated waveguide (SIW) broadband compensating phase shifter," in *IEEE MTT-S Int. Dig.*, Jun. 2009, pp. 845–848.

[23] P. Chen *et al.*, "A multibeam antenna based on substrate integrated waveguide technology for MIMO wireless communications," *IEEE Trans. Antennas Propag.*, vol. 57, no. 6, pp. 1813–1821, Jun. 2009.

[24] R. J. Mailloux, "Reduction of mutual coupling using perfectly conducting fences," *IEEE Trans. Antennas Propag.*, vol. 19, no. 2, pp. 166–173, Mar. 1971.

[25] C. Huang, Z. Zhao, Q. Feng, C. Wang, and X. Luo, "Grooves-assisted surface wave modulation in two-slot array for mutual coupling reduction and gain enhancement," *IEEE Antennas Wireless Propag. Lett.*, vol. 8, pp. 912–915, 2009.

[26] R. J. Mailloux, *Phased Array Antenna Handbook*. Boston, MA, USA: Artech House, 2005.

QING-LING YANG was born in Jiangxi, China, in 1989. He received the B.S. degree from the Chengdu University of Information Technology in 2014. He is currently pursuing the master's degree with the School of Electronic Engineering, University of Electronic Science and Technology of China, Chengdu. His main research interests are millimeter-wave multibeam antenna array with Butler matrix and Rotman lens for 5G wireless communications.

YONG-LING BAN was born in Henan, China. He received the B.S. degree in mathematics from Shandong University in 2000, the M.S. degree in electromagnetics from Peking University in 2003, and the Ph.D. degree in microwave engineering from the University of Electronic Science and Technology of China (UESTC) in 2006. He was a Microwave Engineer with the Xi'an Mechanical and Electric Information Institute in 2006. He was, first, an RF Antenna Design Engineer with Huawei Technologies Company, Ltd., Shenzhen, China, and then a Senior Design Engineer. At Huawei, he designed and implemented various terminal antennas for 15 data card and mobile phone products customized from leading telecommunication industries like Vodafone. Since 2010, he has been an Associate Professor of Microwave Engineering with UESTC. His research interests include wideband small antennas for 4G/5G handset devices, MIMO antenna, and millimeter wave antenna array, in which he has authored over 60 referred journal and conference papers. He holds 20 granted and pending Chinese and overseas patents.
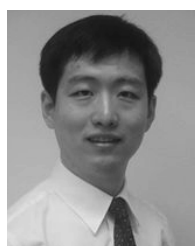
KAI KANG (M'08) received the B.Eng. degree in electrical engineering from Northwestern Polytechnical University, Xi'an, China, in 2002, and the Ph.D. degrees from the National University of Singapore, Singapore, and École Supérieure D'électricité, Gif-sur-Yvette, France, in 2008. From 2006 to 2010, he was a Senior Research Engineer with the Institute of Microelectronics, Agency for Science, Technology and Research, Singapore. From 2009 to 2010, he was an Adjunct Assistant Professor with the National University of Singapore. From 2010 to 2011, he was a Principle Engineer with Global Foundries. Since 2011, he has been with the University of Electronic Science and Technology of China, Chengdu, China, where he is currently a Professor and the Associate Dean of the School of Electronic Engineering. He has authored or co-authored over 80 international refereed journal and conference papers. His research interests are RF and millimeter-wave integrated circuits design and modeling of on-chip devices. He served as the Chapter Chair of the IEEE Solid-State Circuits Society.

CHOW-YEN-DESMOND SIM (M'07–SM'13) was born in Singapore in 1971. He received the B.Sc. degree from the Engineering Department, University of Leicester, U.K., in 1998, and the Ph.D. degree from the Radio System Group, Engineering Department, University of Leicester, in 2003. From 2003 to 2007, he was an Assistant Professor with the Department of Computer and Communication Engineering, Chienkuo Technology University, Changhua, Taiwan. He was an Associate Professor with the Department of Electrical Engineering, Feng Chia University, Taichung, Taiwan, where he became a Full Professor in 2012. He was the Distinguished Chair Professor (Zhiqian Professor) with the School of Communication and Information Engineering, Shanghai University in 2015. He has authored or co-authored over 80 SCI papers. His current research interests include antenna design, VHF/UHF tropospheric propagation, and RFID applications. He is a fellow of the Institute of Engineering and Technology, a Senior Member of the IEEE Antennas and Propagation Society, and a Life Member of the IAET. He received a fee waiver Ph.D. scholarship from the Radio System Group, Engineering Department, University of Leicester, in 1999. He has been serving as the IEEE AP-S Taipei Chapter Chair since 2016. He was the recipient of Best Top 10 Reviewers of IEEE Antenna and Propagation Society for year (2013/2014) and (2014/2015).

GANG WU (M'05) received the B.S. and M.S. degrees in radio communications engineering from the Chongqing University of Post and Telecommunications, Chongqing, China, in 1996 and 1999, respectively, and the Ph.D. degree in communications and information systems from the University of Electronic Science and Technology of China (UESTC), Chengdu, China, in 2004. He was a Lecturer with UESTC in 2004. He was a Research Fellow with the Positioning and Wireless Technology Centre, Nanyang Technological University, Singapore, from 2005 to 2007, and a Visiting Scholar with the Georgia Institute of Technology, Atlanta, GA, USA, from 2009 to 2010. He is currently an Associate Professor with the National Key Laboratory of Science and Technology on Communications, UESTC. His research interest includes MIMO-OFDM, cooperative communications, cognitive radio, resource allocation and scheduling for wireless networks, and energy-efficient wireless networks. He was a Technical Reviewer of dozens of international journals and conferences. He has also been a Technical Program Committee Member of several international conferences. He was an Exemplary Reviewer of the IEEE COMMUNICATIONS LETTERS in 2011 and was a recipient of the IEEE Globecom 2012 Best Paper Award.

• • •